ELSEVIER

Journal of Applied Geophysics 44 (2000) 337–351

JOURNAL OF APPLIED GEOPHYSICS

www.elsevier.nl/locate/jappgeo

Parallel finite element algorithm with domain decomposition for three-dimensional magnetotelluric modelling

Fabio I. Zyserman [a,*], Juan E. Santos [b,c]

[a] *Departamento de Física, Universidad Nacional de La Plata, C.C. 67, 1900 La Plata, Argentina*
[b] *CONICET, Departamento de Geofísica Aplicada, Fac. de Cs., Astronómicas y Geofísicas, U.N.L.P., Paseo del Bosque s/n, 1900 La Plata, Argentina*
[c] *Department of Mathematics, Purdue University, West Lafayette, IN 47907, USA*

Received 13 July 1999; accepted 9 March 2000

Abstract

We present a new finite element (FE) method for magnetotelluric modelling of three-dimensional conductivity structures. Maxwell's equations are treated as a system of first-order partial differential equations for the secondary fields. Absorbing boundary conditions are introduced, minimizing undesired boundary effects and allowing the use of small computational domains. The numerical algorithm presented here is an iterative, domain decomposition procedure employing a nonconforming FE space. It does not use global matrices, therefore allowing the modellization of large and complicated structures. The algorithm is naturally parallellizable, and we show results obtained in the IBM SP2 parallel supercomputer at Purdue University. The accuracy of the numerical method is verified by checking the computed solutions with the results of COMMEMI, the international project on the comparison of modelling methods for electromagnetic induction.

Keywords: Magnetotelluric methods; Numerical models; Finite element analysis; Electromagnetic field; Conductivity

1. Introduction

Numerical modelling of three-dimensional conductivity structures in the earth has experienced a rapid development during the last few years. There are three types of methods that are mostly used, namely integral equation (IE) methods, finite difference (FD) methods and finite element (FE) methods. Among the contributors to the former, we can mention Wannamaker (1991), who extended the capabilities of the integral method to deal with complicated models; Xiong (1992) proposed an iterative method with block partitioning to reduce memory and storage requirements; and Zhdanov and Fang (1996) introduced a quasi-linear approximation for the integral method. The FD has been studied, for example, in Mackie et al. (1993) who solved the integral form of Maxwell's equations, assigning the tangential magnetic field as boundary condition. For the FE, Mogi (1996) used hexahedral elements to calculate

* Corresponding author. Fax: +54-221-4252006.
E-mail address: zyserman@venus.fisica.unlp.edu.ar (F.I. Zyserman).

0926-9851/00/$ - see front matter
PII: S0926-9851(00)00012-4

the secondary fields, and employed asymptotic boundary conditions.

More recently, Zhdanov et al. (1997) presented the results from COMMEMI where different methods of the three classes mentioned above compare their results for standard test models; among them, only one was a FE. It is well-known (Mackie et al., 1993) that FE can more accurately solve complicated structures than IE but up to now it has, for the three-dimensional case, the iron constraint of huge memory requirement for the storage of the global matrices needed to obtain the results.

In the present work, we introduce a hybridized nonconforming iterative domain decomposed mixed finite element procedure (DDFE) (Douglas et al., 2000) to solve Maxwell's equations treated in the form of a system of first-order partial differential equations for the scattered electric and magnetic fields. The boundary conditions employed are first-order absorbing ones (Sheen, 1997), which allow for a significant reduction in the size of the computational domains and are easily introduced into the algorithm. Undesired effects generated by the artificial boundaries, such as reflections, are diminished by these boundary conditions. Besides, because of the domain decomposition approach, no global matrices need to be constructed and only 12×12 linear systems or block diagonal linear systems are solved at each iteration level in each of the subdomains in which the studied region is divided; this feature in turn makes storage requirements smaller. Finally, we mention that the design of the proposed procedure leads to a very efficient parallel code, requiring a small flow of information among processors during the calculations.

In Section 2, we present the model and the differential problem to be solved, and afterwards, we introduce the numerical method. Finally, we show some results of our DDFE, comparing them with those compiled in Zhdanov et al. (1997) and draw the conclusions.

2. The forward differential model

Recall that if $\boldsymbol{E}$ and $\boldsymbol{H}$ denote, respectively, the electric and magnetic fields for a given angular frequency ω, then the time harmonic Maxwell's equations in a region free of sources state that

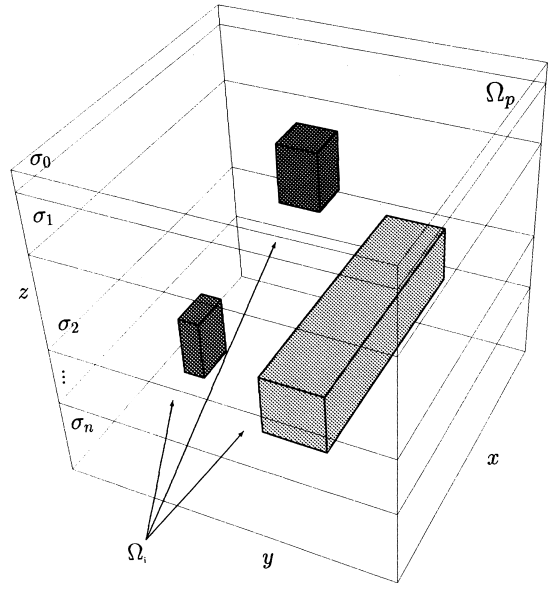

Fig. 1. The 3-D model.

$$\nabla \times \boldsymbol{H} = \sigma \boldsymbol{E}, \tag{1a}$$

$$\nabla \times \boldsymbol{E} = -i\omega\mu \boldsymbol{H}, \tag{1b}$$

where σ and μ denote the electrical conductivity and magnetic permeability, respectively and as it is usual in magnetotellurics, displacement currents have been neglected. Also, associated to Eqs. (1a) and (1b), we have the consistency conditions imposing the continuity of the tangential electric and magnetic fields and the continuity of the current density and magnetic flux normal to any interior interface. Let us consider Eqs. (1a) and (1b) in the three-dimensional domain Ω shown in Fig. 1. The uppermost layer of Ω represents the air, while the others represent a horizontally layered earth with any number of arbitrarily shaped embedded inhomogeneities. The latter must not necessarily lie within a single layer of the former.

According to the description of our domain, the electrical conductivity distribution has the form:

$$\sigma(x,y,z) = \begin{cases} \sigma_p(z) & \text{in } \Omega_p \text{ (layered earth)}, \\ \sigma_p(z) + \sigma_i(x,y,z) & \text{in } \Omega_i \text{ (inhomogeneities)}. \end{cases} \tag{2}$$

In analogy with the 2D case (Wannamaker et al., 1987; Zyserman et al., 1999), we will formulate the differential model in terms of scattered fields. Let the primary electromagnetic fields $\boldsymbol{E}_{\mathrm{p}}$ and $\boldsymbol{H}_{\mathrm{p}}$ be physically meaningful solutions of Maxwell's Eqs. (1a) and (1b) for the horizontally layered model with $\sigma = \sigma_{\mathrm{p}}(z)$. Then, let $\boldsymbol{E}_{\mathrm{t}} = \boldsymbol{E}_{\mathrm{p}} + \boldsymbol{E}_{\mathrm{s}}$ and $\boldsymbol{H}_{\mathrm{t}} = \boldsymbol{H}_{\mathrm{p}} + \boldsymbol{H}_{\mathrm{s}}$ denote the total electromagnetic fields in Ω with conductivity σ as in Eq. (2) induced by a plane, monochromatic electromagnetic wave of frequency ω incident upon its top boundary. Finally, let $\boldsymbol{E}_{\mathrm{s}}$ and $\boldsymbol{H}_{\mathrm{s}}$ be the scattered electromagnetic fields due to the presence of the conductivity anomalies Ω_{i}; they satisfy the equations

$$\sigma \boldsymbol{E}_{\mathrm{s}} - \nabla \times \boldsymbol{H}_{\mathrm{s}} = -\sigma_{\mathrm{i}} \boldsymbol{E}_{\mathrm{p}} = -\boldsymbol{F}, \tag{3a}$$

$$i\omega\mu \boldsymbol{H}_{\mathrm{s}} + \nabla \times \boldsymbol{E}_{\mathrm{s}} = 0. \tag{3b}$$

which are the ones we are going to deal with. In order to minimize the effect of the artificial boundaries, we will use the absorbing boundary condition introduced by (Sheen, 1997):

$$(1-i) P_\tau a \boldsymbol{E}_{\mathrm{s}} + \nu \times \boldsymbol{H}_{\mathrm{s}} = 0 \quad \text{on } \partial\Omega \equiv \Gamma, \tag{4}$$

where $a = (\sigma/2\omega\mu)^{1/2}$ Here, ν is the unit outer normal to Γ, the boundary of the domain Ω, and $P_\tau \varphi = \varphi - \nu(\nu \cdot \varphi) = -\nu \times (\nu * \varphi)$. For the sake of simplicity, from now on we will omit the subscripts for the secondary fields.

Let us briefly comment on the meaning of Eq. (4). Our aim is to simulate, as close as possible, the vanishing of the electromagnetic field at infinity, but considering a finite domain. On choosing, e.g., a Dirichlet boundary condition on Γ, one must extend the domain until the fields are negligible, leading to the use of large computational domains at the cost of increasing CPU times and memory requirements. On the other hand, by using Eq. (4), we make a field normally 'arriving' to the border Γ to be 'absorbed' by it, i.e., we make it leave our domain with no reflections; and this can be done relatively close to the inhomogeneities.

Next, we proceed to describe the *domain decomposition* procedure. Let us consider a partition of our original domain Ω into non-overlapping — not necessarily homogeneous — parallelepipeds Ω_j of volume $h_{x_j} \times h_{y_j} \times h_{z_j}$, $j = 1, \ldots, J$. Let Γ_j be the boundary of the subdomain Ω_j, consisting of six rectangles, namely $\Gamma_j = \{\mathscr{F}\text{ront}, \mathscr{B}\text{ack}, \mathscr{W}\text{est}, \mathscr{E}\text{ast}, \mathscr{N}\text{orth}, \mathscr{S}\text{outh}\}$ (to avoid cumbersome notation, the subindex j associated with each rectangle in Γ_j is omitted). In each subdomain Ω_j, Eqs. (3)–(4) become:

$$\sigma \boldsymbol{E}_j - \nabla \times \boldsymbol{H}_j = -(\sigma_{\mathrm{i}})_j \boldsymbol{E}_{\mathrm{p}} = -\boldsymbol{F}_j, \tag{5a}$$

$$i\omega\mu \boldsymbol{H}_j + \nabla \times \boldsymbol{E}_j = 0, \tag{5b}$$

and

$$(1-i) P_\tau a_j \boldsymbol{E}_j + \nu \times \boldsymbol{H}_j = 0 \quad \text{on } B_j. \tag{6}$$

Here B_{j} stands for the intersection of the boundary of the domain Ω_j with Γ. Clearly, consistency conditions need to be imposed on all interior boundaries; (i.e., on all rectangles building Γ_j such that their intersection with Γ is empty). The natural conditions are given, as already stated, by the continuity of the tangential electric and magnetic fields on these boundaries:

$$\nu_j \times \boldsymbol{H}_j = -\nu_k \times \boldsymbol{H}_k \quad \text{on } \Gamma_{jk}, \tag{7a}$$

$$P_\tau \boldsymbol{E}_j = P_\tau \boldsymbol{E}_k \quad \text{on } \Gamma_{jk}. \tag{7b}$$

In the above equations Γ_{jk} stands for the face shared by the adjacent domains Ω_j and Ω_k. Of course, $\Gamma_{jk} = \Gamma_{kj}$, but care must be taken when considering the direction of the normal vector to the face, i.e., Γ_{jk} is the face as seen from Ω_j and Γ_{kj} is the same face but as seen from Ω_k. For the iterative algorithm to be defined below, it is more convenient (Douglas et al., 1993) to replace Eqs. (7a) and (7b) by the equivalent Robin-type transmission conditions:

$$\nu_j \times \boldsymbol{H}_j = -\nu_k \times \boldsymbol{H}_k - \beta_{jk}\left(P_\tau \boldsymbol{E}_j - P_\tau \boldsymbol{E}_k\right) \quad \text{on } \Gamma_{jk} \subset \Gamma_j, \tag{8a}$$

$$\nu_k \times \boldsymbol{H}_k = -\nu_j \times \boldsymbol{H}_j - \beta_{jk}\left(P_\tau \boldsymbol{E}_k - P_\tau \boldsymbol{E}_j\right) \quad \text{on } \Gamma_{kj} \subset \Gamma_k, \tag{8b}$$

Here, β_{jk} is a complex parameter defined on the interfaces Γ_{jk} with a positive real part and a negative imaginary part. In Appendix A, we explain how we chose its values.

To obtain a variational formulation for Eqs. (5)–(6), we proceed as usual (Douglas et al., 1997; Martinec, 1997). We test Eq. (5a) with real vector functions $\varphi(x,y,z)$ such that $\nabla \times \varphi(x,y,z)$ is square integrable; and Eq. (5b) by square integrable real vector functions $\psi(x,y,z)$ (Santos and Sheen, 1998).

Using integration by parts in the terms involving the curl of the magnetic field, and applying the Robin transmission boundary conditions (8a) and (8b) for the *interior* boundaries and the absorbing boundary condition (6) on B_j, we obtain the equations:

$$\int_{\Omega_j} \sigma \boldsymbol{E}_j \varphi \mathrm{d}^3x - \int_{\Omega_j} \boldsymbol{H}_j \nabla \times \varphi \mathrm{d}^3x + \sum_k \int_{\Gamma_{jk}} \left(\beta_{jk} \left(P_\tau \boldsymbol{E}_j - P_\tau \boldsymbol{E}_k \right) + \nu_k \times \boldsymbol{H}_k \right) P_\tau \varphi \mathrm{d}S + (1-i) \int_{B_j} P_\tau a \boldsymbol{E}_j P_\tau \varphi \mathrm{d}S = -\int_{\Omega_j} \boldsymbol{F}_j \varphi \mathrm{d}^3x, \tag{9a}$$

$$i\omega\mu \int_{\Omega_j} \boldsymbol{H}_j \psi \mathrm{d}^3x + \int_{\Omega_j} \nabla \times \boldsymbol{E}_j \psi \mathrm{d}^3x = 0. \tag{9b}$$

The sum in the third term in the left-hand side of the first equation runs over the rectangles Γ_{jk} building the interface among Ω_j and its neighbours; whenever Γ_{jk} is also part of Γ, the contribution of the corresponding integral is neglected. On the other hand, the contribution of the last term on the left-hand side of Eq. (9a) is different from zero only when the integration is done on a rectangle that is simultaneously part of the boundary of the computational domain Ω.

The idea of the domain decomposition procedure is to solve the posed problem separately in each subdomain Ω_j. Taking into account that Eqs. (8a) and (8b) involves only subdomains adjacent to Ω_j, we propose the following iterative algorithm:

1. Choose initial values $(\boldsymbol{E}^0, \boldsymbol{H}^0)$
2. Compute $(\boldsymbol{E}^{n+1}, \boldsymbol{H}^{n+1})$ as the solution of the equations

$$\int_{\Omega_j} \sigma_j \boldsymbol{E}_j^{n+1} \varphi \mathrm{d}^3x - \int_{\Omega_j} \boldsymbol{H}_j^{n+1} \nabla \times \varphi \mathrm{d}^3x + \sum_k \int_{\Gamma_{jk}} \beta_{jk} P_\tau \boldsymbol{E}_j^{n+1} P_\tau \varphi \mathrm{d}S + (1-i) \int_{B_j} P_\tau a_j \boldsymbol{E}_j^{n+1} P_\tau \varphi \mathrm{d}S = -\int_{\Omega_j} \boldsymbol{F}_j \varphi \mathrm{d}^3x + \sum_k \int_{\Gamma_{jk}} \left(\beta_{jk} P_\tau \boldsymbol{E}_k^n - \nu_k \times \boldsymbol{H}_k^n \right) P_\tau \varphi \mathrm{d}S \tag{10a}$$

$$i\omega\mu \int_{\Omega_j} \boldsymbol{H}_j^{n+1} \psi \mathrm{d}^3x + \int_{\Omega_j} \nabla \times \boldsymbol{E}_j^{n+1} \psi \mathrm{d}^3x = 0, \tag{10b}$$

$$\nu_j \times \boldsymbol{H}_j^{n+1} = -\nu_k \times \boldsymbol{H}_k^n - \beta_{jk} \left(P_\tau \boldsymbol{E}_j^{n+1} - P_\tau \boldsymbol{E}_k^n \right) \text{ on } \Gamma_{jk}. \tag{10c}$$

We point out that for the subdomain Ω_j, the right-hand side of Eq. (10a) contains unknowns belonging to its neighbour cells, and they are one iteration step behind, i.e., they are assumed to be data at the current iteration level. In Section 3, we will define the discrete procedure motivated by the above iteration.

3. The finite element procedure

In order to simplify the description of the numerical procedure, we will assume that the domain decomposition partition (the already mentioned paralellepipeds Ω_j) of the domain Ω coincides with the FE partition. Later, we will briefly indicate the changes for the case in which the subdomains consist of strips in the x-direction.

In each cell Ω_j, we approximate the electric and magnetic fields, respectively, by the expressions:

$$\boldsymbol{E}_j = \sum_\alpha \varepsilon_j^{\alpha, n+1} \varphi^\alpha \left(\frac{2x}{h_x} - 1, \frac{2y}{h_y} - 1, \frac{2z}{h_z} - 1 \right),$$

$$\boldsymbol{H}_j = \sum_\eta h_j^{\eta, n+1} \psi^\eta \left(\frac{2x}{h_x} - 1, \frac{2y}{h_y} - 1, \frac{2z}{h_z} - 1 \right), \tag{11}$$

where the superscripts α and η cover all the corresponding basis functions given in Table 1, and the complex coefficients $\varepsilon_j^{\alpha, n+1}$ and $h_j^{\eta, n+1}$ need to be determined at the iteration level $n+1$. Therefore, we use 12 basis functions for $\boldsymbol{E}_j$ and nine basis functions for $\boldsymbol{H}_j$. The scaling and translation of the basis functions φ^α and ψ^η in Eq. (11) is made in order to keep the variables within the reference element $[-1,1]^3$. In Fig. 2, the reference cube and relation among coefficients belonging to adjacent paralellepipeds is shown. The dependence of the lengths h_x, h_y and h_z on the index j was omitted for simplicity in the notation.

Table 1
The nonconforming FE basis functions for $\boldsymbol{E}$ and $\boldsymbol{H}$, defined in $[-1,1]^3$ (see Fig. 2 for details on the reference cube). Let us consider, to clarify ideas, the first basis function for the electric field. The only nonzero component of this vector function, i.e., the x-component, takes the value 1 on the mid-point of the $\mathscr{W}$ face, and zero on the mid-points of all other faces. The other basis functions display similar behaviour. It can also be seen that the space spanned by the functions ψ^{η} is the curl of the one spanned by the functions φ^{α}, as usual requirement for mixed methods. The selected basis functions also make it possible to obtain as estimate on the rate of convergence of the proposed algorithm in terms of the mesh size (Douglas et al., 2000)

α	φ^{α}	η	ψ^{η}
$\mathscr{W}_x$	$(1/4-y/2-3/8(y^2-(5/3)y^4-(z^2-(5/3)z^4)),0,0)$	1	$(1/8,0,0)$
$\mathscr{E}_x$	$(1/4+y/2-3/8(y^2-(5/3)y^4-(z^2-(5/3)z^4)),0,0)$	2	$(3/56(y-(10/3)y^3),0,0)$
$\mathscr{S}_x$	$(1/4-z/2+3/8(y^2-(5/3)y^4-(z^2-(5/3)z^4)),0,0)$	3	$(-3/56(z-(10/3)z^3),0,0)$
$\mathscr{N}_x$	$(1/4+z/2+3/8(y^2-(5/3)y^4-(z^2-(5/3)z^4)),0,0)$	4	$(0,1/8,0)$
$\mathscr{B}_y$	$(0,1/4-x/2-3/8(x^2-(5/3)x^4-(z^2-(5/3)z^4)),0)$	5	$(0,-3/56(x-(10/3)x^3),0)$
$\mathscr{F}_y$	$(0,1/4+x/2-3/8(x^2-(5/3)x^4-(z^2-(5/3)z^4)),0)$	6	$(0,3/56(z-(10/3)z^3),0)$
$\mathscr{W}_z$	$(0,0,1/4-y/2+3/8(x^2-(5/3)x^4-(y^2-(5/3)y^4)))$	7	$(0,0,1/8)$
$\mathscr{E}_z$	$(0,0,1/4+y/2+3/8(x^2-(5/3)x^4-(y^2-(5/3)y^4)))$	8	$(0,0,3/56(x-(10/3)x^3))$
$\mathscr{S}_y$	$(0,1/4-z/2+3/8(x^2-(5/3)x^4-(z^2-(5/3)z^4)),0)$	9	$(0,0,-3/56(y-(10/3)y^3))$
$\mathscr{N}_y$	$(0,1/4+z/2+3/8(x^2-(5/3)x^4-(z^2-(5/3)z^4)),0)$		
$\mathscr{B}_z$	$(0,0,1/4-x/2-3/8(x^2-(5/3)x^4-(y^2-(5/3)y^4)))$		
$\mathscr{F}_z$	$(0,0,1/4+x/2-3/8(x^2-(5/3)x^4-(y^2-(5/3)y^4)))$		

The next step is to *hybridize* (Arnold and Brezzi, 1985) the algorithm to make the algebraic problem easier. This is achieved by eliminating the constraint requiring the continuity of the tangential components of the electric field on the faces Γ_{jk}, and enforcing instead the required continuity through Lagrange multipliers defined at the interelement boundaries Γ_{jk}. Furthemore, as an additional simplification, instead of applying the continuity of these tangential components on the whole interface Γ_{jk}, we will impose it only at the mid-points m_{jk} of Γ_{jk}. The introduction of the Lagrange multipliers allows for a simplification of the associated algebraic problem, which becomes block diagonal and consequently, the approximate electric and magnetic fields can be separately computed. Thus, for each one of the rectangles building Γ_j that are not part of the boundary Γ, we introduce a two-dimensional constant vector or Lagrange multiplier λ_{jk}^{n+1} associated with the value of $\nu_j \times \boldsymbol{H}_j^{n+1}$ at the mid-point m_{jk} of the face Γ_{jk}, i.e., we will have an additional two-dimensional unknown vector λ_{jk}^{n+1} per each face of the domain Ω_j.

Therefore, Eq. (10c) becomes:

$$\lambda_{jk}^{n+1} = -\lambda_{kj}^{n} - \beta_{jk}\left(P_{\tau}\boldsymbol{E}_j^{n+1}(m_{jk}) - P_{\tau}\boldsymbol{E}_k^{n}(m_{jk})\right) \text{ on } \Gamma_{jk}. \quad (12)$$

Note that as stated above, Eq. (12) imposes the continuity of the tangential components of the electric field *only* at the mid-points m_{jk} of the faces Γ_{jk}. Also, accordingly with what we just mentioned, the expression $\nu_k \times \boldsymbol{H}_k^n$ in the last integral of the right-hand side of Eq. (10a) is replaced by the Lagrange multiplier λ_{kj}^n.

To get the algebraic form of Eqs. (10a)–(10c), the fields $\boldsymbol{E}_j$ and $\boldsymbol{H}_j$ as defined in Eq. (11) are replaced in Eqs. (10a) and (10b). Then, the functions φ^{α} and ψ^{η} scaled as in Eq. (11) are taken as test functions in Eqs. (10a) and (10b), respectively, in the order given in Table 1. The surface integrals in Eqs. (10a)–(10c) were approximated by the mid-point rule, i.e., we used $\int_A fg\,\mathrm{d}S \approx |A| f(m) g(m)$, where $|A|$ is the area of the surface A, and m is its mid-point.

This task yields a 21×21 linear system of equations for each subdomain Ω_j, at each iteration level. The problem can be further simplified because the choice of the basis functions for the magnetic field allows to get the coefficients $h_j^{\eta,n+1}$ in terms of the coefficients $\varepsilon_j^{\alpha,n+1}$, by using the set of linear equations rendered by Eq. (10b). Once this simple algebra is carried out, we end up with a 12×12 linear system of the form $C_j\ \varepsilon_j^{n+1} = b_j^n$. The coefficient matrices C_j remain unchanged along the iterative process whereas the vectors b_j^n must be recalculated at each iteration; in Appendix A, the linear system is

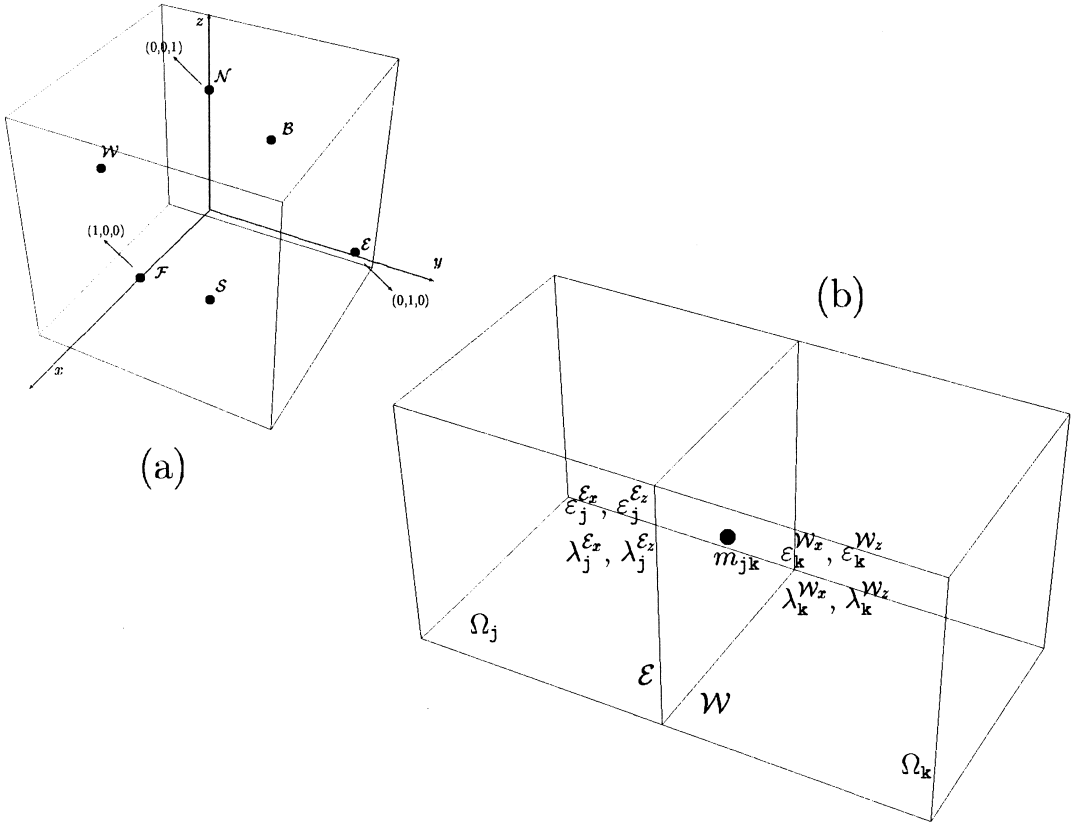

Fig. 2. (a) Display of the reference cube $[-1, 1]^3$. We associate the coefficients of the electric field with the mid-points of the faces of the cube, where the single nonzero component of the respective basis functions takes the value 1. The degrees of the freedom of H are obtained from momenta, therefore there is no specific position associated with them in the reference cube. (b) Continuity of the electric field is asked, as stated in Eq. (12), only in the mid-point m_{jk} of the face. Displayed coefficients ε, which are the only ones involved in this interface, asymptotically verify this condition. Also, because of Eq. (12), we have that the equations $\lambda_j^{\mathcal{E}_x} = -\lambda_k^{\mathcal{W}_x}$ and $\lambda_j^{\mathcal{E}_t} = -\lambda_k^{\mathcal{W}_z}$ hold asymptotically, or equivalently, we have continuity of the tangential components of the magnetic field at the mid-point of the interface asymptotically. Similar is the situation for the other faces.

explicitly shown. The last task is to get the discrete version of Eq. (12), which is easily accomplished using Eq. (11).

We can therefore state our iterative algorithm as follows:

1. Choose initial values $(\varepsilon_j^{\alpha,0},\ \lambda_{jk}^0)$ for the unknowns in all cells Ω_j.
2. For all domains Ω_j
   Solve the 12×12 linear system for the unknowns $\varepsilon_j^{\alpha,n+1}$.
   Compute λ_{jk}^{n+1}.
3. Check for convergence. If it has not been achieved, go to step 2.

As is usual for iterative algorithms, convergence is reached when the relative error of the calculated coefficients is smaller than a prescribed tolerance, i.e., when within this tolerance the coefficients have stopped changing. At this stage, the unknowns h_j^η can be easily calculated as indicated above.

We note that the convergence of the above iterative procedure to the solution of the original differential problems (3)–(4) has been demonstrated in Douglas et al. (2000). More specifically, in the mentioned reference, it has been shown that the difference between the solution of (3)–(4) and the solution of the presented iterative procedure is asymptotically of order $h^{1/2}$, where h is the mesh size. We also

wish to point out that after the convergence of the iterative procedure has been achieved, since the continuity of the electric field is imposed only at the mid-points of the interfaces and *not* on the whole interfaces as in the standard conforming FE methods (Nedelec, 1980, 1982; Santos and Sheen, 1998), the algorithm yields an approximate solution which is nonconforming, i.e, the approximate electric field has no square integrable curl as it is the case for the electric field in the original differential problems (3)–(4).

We also implemented the iterative domain decomposition procedure for the case in which the subdomains are strips in the x-direction, each of them consisting of a number n_x of parallelepipeds Ω_j. The representation Eq. (11) was changed so that within a strip, there are just two coefficients of the electric field associated to the interface back–front of two adjacent parallelepipeds. (We assume that the faces $\mathscr{F}$ and $\mathscr{B}$ of the parallelepipeds in any strip are normal to the x-axis). Consequently, the resulting linear system for the electric field is block diagonal — two cells share the same two coefficients — and the number of unknowns is $10n_x + 2$. If the original number of subdomains was, for example, $n_x n_y n_z$, with this change we have $n_y n_z$ linear systems of the order given above, still much simpler to deal with than a unique global matrix. Of course, the right-hand side of the linear system has to be changed accordingly. With the strips structure, it is possible to apply a red–black procedure (Douglas et al., 1997; Zyserman et al., 1999), which yields a reduction of about 50% in the number of iterations needed to reach a given tolerance for the relative error.

Let us now describe how the algorithm works on a parallel computer. For the implementation of the parallel code, we used the MPI standard (Pacheco, 1997), which makes it portable to any platform. The most efficient way to perform the calculations is to assign to each processor, as close as possible, the same number of unknowns (Alumbaugh et al., 1996). In our case, that means to assign the same number of subdomains Ω_j to each processor. If the load of the processors is not balanced, some will remain idle while others are still computing, reducing the efficiency of the algorithm. In order to fix ideas, let us work with four processors. Each one runs exactly the same copy of the program, and gets the input data from a single data file. Local variables are converted to global when necessary within the code; we preferred this strategy to splitting the input file in

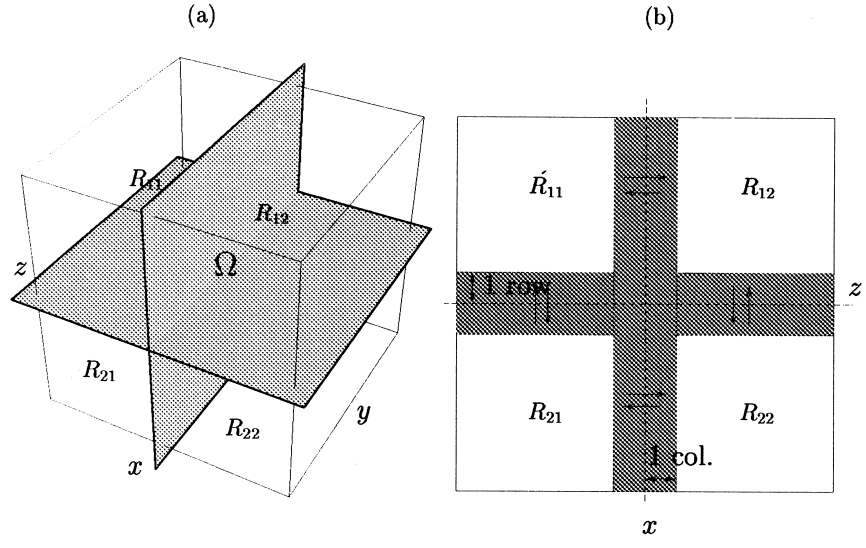

Fig. 3. (a) Scheme of the division of the domain Ω among processors. (b) Flow of information among processors, the shaded areas represent the subdomains involved in the process. Only a single column (row) of cells adjacent to the virtual boundary participates in the process.

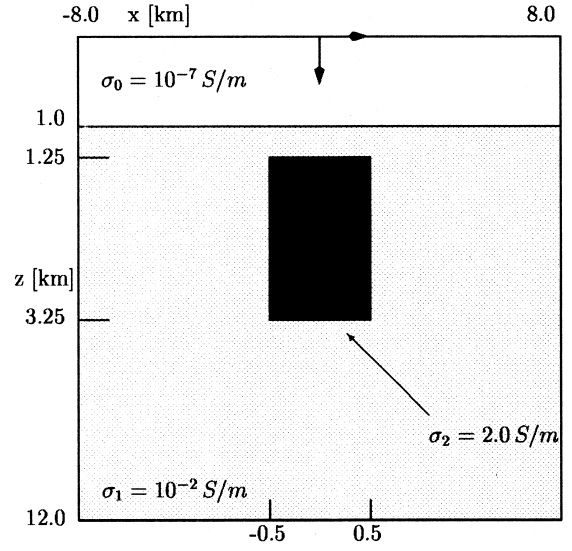

Fig. 4. A 2-D slice of Model 1 at $y = 0$. The anomaly measures 2 km in the y direction.

multiple ones to be read by each processor (Newman and Alumbaugh, 1997). In Fig. 3a, the planes represent the virtual boundaries created by assigning a portion of the domain Ω to each processor. Naturally, it is possible to do this assignment in different ways, we chose the displayed one. The processor number 1 solves the DDFE only in R_{11}, and simultaneously, the other processors perform their calculations in their respective regions.

The time needed to get the solution is usually longer than one-fourth of the time with a serial code on one processor (assuming that processors of the same kind are used). This happens because on each iteration level 'adjacent' processors must interchange information, so that step 2 of the proposed algorithm is adequately performed: In Fig. 3b (a slice of Fig. 3a for constant y), the shaded regions of R_{12} to the right of the vertical virtual boundary and of R_{21} below the horizontal one involve just one column and one row, respectively of cells neighbour to subdomains in R_{11}. Therefore, all the coefficients $\varepsilon^{\alpha,n}$ and λ^n associated with the aforementioned row and column must be sent to processor number 1 in order to build the corresponding right-hand side vec-

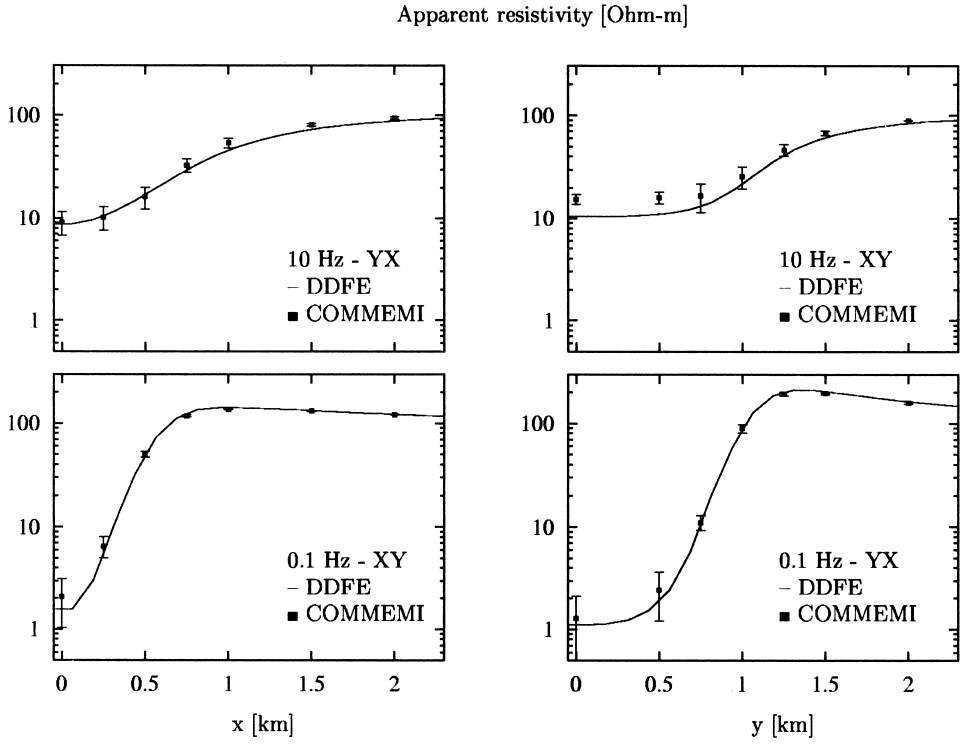

Fig. 5. Results for Model 1.

Table 2
Performance on the IBM SP/2 for the presented models

	CPU time [s]			
Processors	1	4	8	16
Model 1, *YX*-mode, 10 Hz	1867.2	338.71	164.96	78.96
Model 2, *YX*-mode, 10^{-3} Hz	6948.71	1370.94	632.87	329.05

tors b^n. Clearly, the same is valid for the other three regions; the interchange of information among processors is simultaneously done at the end of step 2.

We asserted that the DDFE is naturally parallelizable not only because of the description given above, but also due to the fact that the amount of data to be transferred is not large. As sketched in Fig. 3b, the shaded region lies on only a single subdomain width. It is easily seen that the flow of information grows with the number of processors. Therefore, the efficiency of the algorithm reaches its peak for some number of them, and beyond that number, it becomes useless to employ more. However, for the number of processors available (16), we did not experience this situation in our calculations.

4. Synthetic examples

We present results of two models suggested in the COMMEMI project (Zhdanov et al., 1997). The first one (Model 1) is displayed in Fig. 4; it consists of a conductive block of 2 S/m embedded in a homogeneous Earth with conductivity 0.01 S/m. The anomaly measures $1 \times 2 \times 2$ km. We set the dimensions of our computational domain to be $16 \times 16 \times 12$ km; an air layer measuring 1 km in height and with conductivity $\sigma_0 = 10^{-7}$ S/m was included. The absorbing boundary condition employed makes it unnecessary to use a thicker air layer; this assertion is supported by performed numerical tests.

A $58 \times 64 \times 32$-element inhomogeneous grid was used for this model, the smallest elements were of course located within and around the inhomogeneity. Two frequencies were considered: 10 Hz to test the algorithm in the presence of strongly damped fields, and 0.1 Hz to check if the numerical procedure can cope with the stationary component of the solution; this case is also useful to study the boundary condition behaviour.

To test our algorithm, we show two principal apparent resistivities, ρ_{xy} and ρ_{yx}, corresponding to polarizations $\boldsymbol{E} = (E,0,0)$, $\boldsymbol{H} = (0,H,0)$ (*XY*-mode) and $\boldsymbol{E} = (0,E,0)$, $\boldsymbol{H} = (H,0,0)$ (*YX*-mode), respectively. The results of the above-mentioned work are presented as error bars; taking as mid-points the means of the data after rejecting outliers, the bars measure $2\delta_1$, twice the standard deviation of the reduced data set.

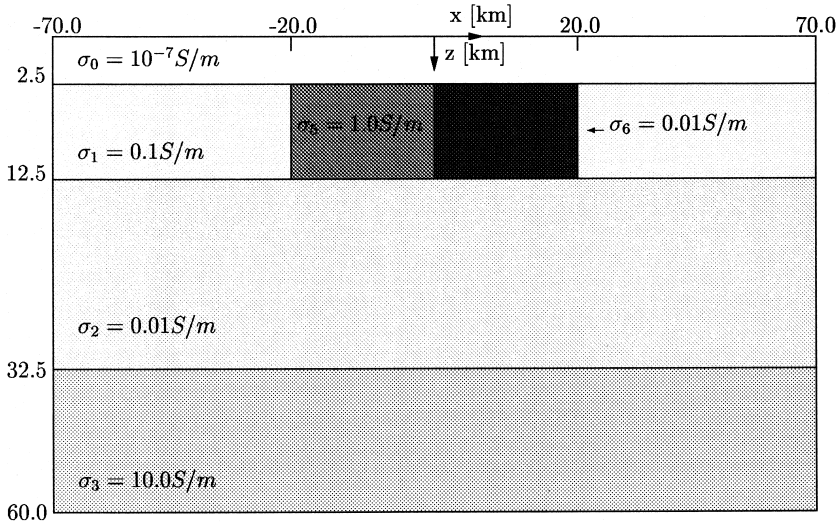

Fig. 6. Model 2.

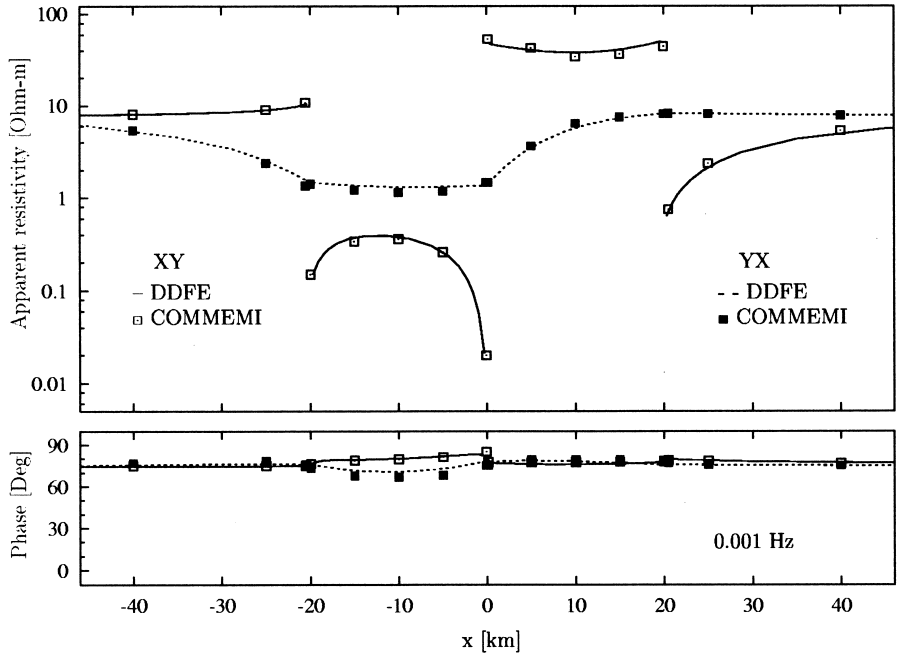

Fig. 7. Apparent resistivity and impedance phase measured on the surface of the earth, slice at $y = 0$. Agreement between both results is very good.

The tolerance for the relative error was set to 10^{-4} in all cases. The number of iterations to reach convergence strongly depends on the mode and the frequency: 104 for the *YX*-mode at 10 Hz, to 457 for

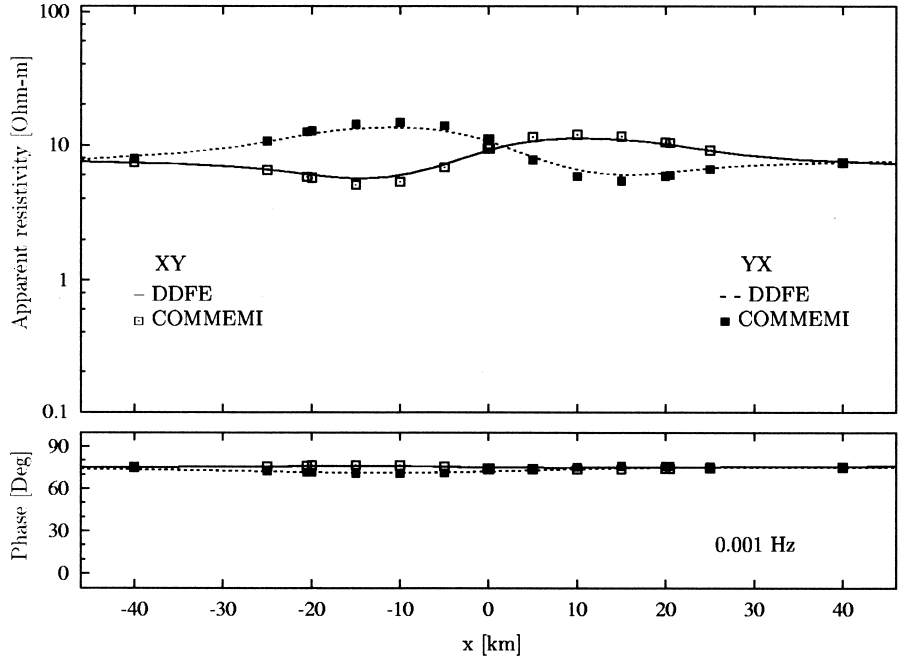

Fig. 8. Same as Fig. 7, slice at $y = 30$.

the same mode at 0.1 Hz. The results obtained are, in general, in very good agreement with those of the referenced paper, as can be seen in Fig. 5. The two graphs situated on the left side of the figure show measurements along the x-axis for $y = 0$; the two graphs on the right side display measurements made along the y-axis for $x = 0$. Finally, in Table 2, we display the performance of our algorithm on an SP2 parallel supercomputer at Purdue University. The results correspond to the *YX*-mode at 10 Hz.

The second model we solved (Model 2) is shown in Fig. 6. It consists of two blocks of $20 \times 40 \times 10$ km with conductivities $\sigma = 1.0$ S/m and $\sigma = 0.01$ S/m immersed in a three-layered earth with depths of 10, 20, and 27.5 km. The upper layer, where the blocks lie, has conductivity $\sigma = 0.1$ S/m, i.e., the two blocks are chosen to be conductive and resistive, respectively, compared to their host. For the second and third layers, the conductivity values were chosen to be $\sigma = 0.01$ and 10.0 S/m, respectively. The air layer thickness is 2.5 km, therefore, the domain as a whole comprises $140 \times 120 \times 60$ km. As in the former case, we chose $\sigma = 10^{-7}$ S/m for the air layer conductivity.

Contrary to Model 1 for which many results obtained with different methods were submitted, for Model 2 just one author sent data — obtained with an integral method. We have already mentioned other existing solutions for this model (Mackie et al., 1993), but we are not aware of any solution provided by FE methods.

The results we show in Figs. 7 and 8 — 2D slices for $y = 0$ and 30 km, respectively — were obtained with an inhomogeneous grid of $54 \times 54 \times 32$ elements, and relative error tolerance of 10^{-4} at a frequency of 10^{-3} Hz.

5. Conclusions

We have presented an iterative finite element method for solving the forward three-dimensional magnetotelluric problem. The method has many interesting features, among them we can mention (a) the nonconforming finite element basis chosen that allows us to write the unknowns corresponding to the magnetic field in terms of the ones of the electric field; and minimizes the amount of information transferred among processors; (b) the domain decomposition approach that makes it possible to work with small matrices, minimizing storage and memory requirements; (c) the absorbing boundary conditions introduced proved to perform very well, making it possible to work with relatively small computational domains without introducing inaccuracies; (d) the method is naturally parallellizable, therefore making the solution of large and complicated models possible.

Acknowledgements

The authors wish to thank the SuperComputing Center of Purdue University, and the RHRK, University of Kaiserslautern, for providing CPU time and technical advice. This work was financially supported by the Agencia Nacional de Promoción Científica y Tecnológica under contract BID-802/OC-AR. Many thanks to Peter Weidelft and Phil Wannamaker for reviews.

Appendix A

Here we show the final form of the 12×12 linear system to be solved in each of the subdomains in which we divide the domain Ω. Throughout this appendix we assume we have $n_x \cdot n_y \cdot n_z$ subdomains; and to clearly state the algebraic problem associated with the iterative procedure, it is more convenient to number the subdomains Ω_j and all variables with three indices *rst*. Therefore, the subdomains neighbouring to Ω_{rst} are those with one subscript increased or decreased by one.

We will also change the notation for the coefficients defined on the faces Γ_{rst}. For example, for the front face $\mathcal{F}$ of Ω_{rst} Eq. (12) becomes:

$$\lambda_{rst}^{\mathcal{F},n+1} = -\lambda_{r-1st}^{\mathcal{B},n} - \beta_{rst}^{\mathcal{F}}\left(P_\tau \boldsymbol{E}_{rst}^{n+1}\left(m_{rst}^{\mathcal{F}}\right) - P_\tau \boldsymbol{E}_{r-1st}^{n}\left(m_{rst}^{\mathcal{F}}\right)\right).$$

The coefficient matrix C is symmetric, the structure shown is obtained by replacing the test functions

in Eq. (10a) by the basis functions in the order given in Table 1, and replacing the coefficients for the magnetic field in term of the ones of the electric field obtained from Eq. (10b).

$$\mathbf{C}=\begin{pmatrix} c_{11} & c_{12} & c_{13} & c_{14} & c_{15} & c_{16} & 0 & 0 & 0 & 0 & 0 & 0 \\ & c_{22} & c_{23} & c_{24} & c_{25} & c_{26} & 0 & 0 & 0 & 0 & 0 & 0 \\ & & c_{33} & c_{34} & 0 & 0 & 0 & 0 & 0 & 0 & c_{3\,11} & c_{3\,12} \\ & & & c_{44} & 0 & 0 & 0 & 0 & 0 & 0 & c_{4\,11} & c_{4\,12} \\ & & & & c_{55} & c_{56} & 0 & 0 & c_{59} & c_{5\,10} & 0 & 0 \\ & & & & & c_{66} & 0 & 0 & c_{69} & c_{6\,10} & 0 & 0 \\ & & & & & & c_{77} & c_{78} & c_{79} & c_{7\,10} & c_{7\,11} & c_{7\,12} \\ & & & & & & & c_{88} & c_{89} & c_{8\,10} & c_{8\,11} & c_{8\,12} \\ & & & & & & & & c_{99} & c_{9\,10} & 0 & 0 \\ & & & & & & & & & c_{10\,10} & 0 & 0 \\ & & & & & & & & & & c_{11\,11} & c_{11\,12} \\ & & & & & & & & & & & c_{12\,12} \end{pmatrix}$$

where

$$c_{11}=\frac{781}{5040}h_x h_y h_z \sigma_{rst}+\frac{1}{i\omega\mu}\left(\frac{1036}{784}\left(\frac{h_x h_y}{h_z}+\frac{h_x h_z}{h_y}\right)+\frac{h_x h_z}{h_y}\right)+h_x h_z(1-\delta_{s1})\beta^{\mathscr{W}}_{rst}+(1-i)\delta_{s1}h_x h_z a_{rst},$$

$$c_{12}=\frac{-59}{5040}h_x h_y h_z \sigma_{rst}+\frac{1}{i\omega\mu}\left(\frac{1036}{784}\left(\frac{h_x h_y}{h_z}+\frac{h_x h_z}{h_y}\right)-\frac{h_x h_z}{h_y}\right),$$

$$c_{13}=\frac{269}{5040}h_x h_y h_z \sigma_{rst}-\frac{1}{i\omega\mu}\frac{1036}{784}\left(\frac{h_x h_y}{h_z}+\frac{h_x h_z}{h_y}\right),$$

$$c_{14}=c_{13},$$

$$c_{15}=-\frac{1}{i\omega\mu}h_z,$$

$$c_{16}=\frac{1}{i\omega\mu}h_z,$$

$$c_{22}=\frac{781}{5040}h_x h_y h_z \sigma_{rst}+\frac{1}{i\omega\mu}\left(\frac{1036}{784}\left(\frac{h_x h_y}{h_z}+\frac{h_x h_z}{h_y}\right)+\frac{h_x h_z}{h_y}\right)+h_x h_z\left(1-\delta_{sn_y}\right)\beta^{\mathscr{E}}_{rst}+(1-i)\delta_{sn_y}h_x h_z a_{rst},$$

$$c_{23}=c_{13},$$

$$c_{24}=c_{14},$$

$$c_{25}=c_{16},$$

$$c_{26}=c_{15},$$

$$c_{33}=\frac{781}{5040}h_x h_y h_z \sigma_{rst}+\frac{1}{i\omega\mu}\left(\frac{1036}{784}\left(\frac{h_x h_y}{h_z}+\frac{h_x h_z}{h_y}\right)+\frac{h_x h_y}{h_z}\right)+h_x h_y(1-\delta_{t1})\beta^{\mathscr{S}}_{rst}+(1-i)\delta_{t1}h_x h_y a_{rst},$$

$$c_{34}=\frac{-59}{5040}h_x h_y h_z \sigma_{rst}+\frac{1}{i\omega\mu}\left(\frac{1036}{784}\left(\frac{h_x h_y}{h_z}+\frac{h_x h_z}{h_y}\right)-\frac{h_x h_y}{h_z}\right),$$

$$c_{3\,11} = -\frac{1}{i\omega\mu}h_y,$$

$$c_{3\,12} = \frac{1}{i\omega\mu}h_y,$$

$$c_{44} = \frac{781}{5040}h_x h_y h_z \sigma_{rst} + \frac{1}{i\omega\mu}\left(\frac{1036}{784}\left(\frac{h_x h_y}{h_z} + \frac{h_x h_z}{h_y}\right) + \frac{h_x h_y}{h_z}\right) + h_x h_y\left(1-\delta_{tn_z}\right)\beta^{\mathscr{N}}_{rst} + (1-i)\,\delta_{tn_z}h_x h_y a_{rst},$$

$$c_{4\,11} = c_{3\,11},$$

$$c_{4\,12} = c_{3\,12},$$

$$c_{55} = \frac{781}{5040}h_x h_y h_z \sigma_{rst} + \frac{1}{i\omega\mu}\left(\frac{1036}{784}\left(\frac{h_x h_y}{h_z} + \frac{h_y h_z}{h_x}\right) + \frac{h_y h_z}{h_x}\right) + h_y h_z(1-\delta_{r1})\,\beta^{\mathscr{B}}_{rst} + (1-i)\,\delta_{r1}h_y h_z a_{rst},$$

$$c_{56} = \frac{-59}{5040}h_x h_y h_z \sigma_{rst} + \frac{1}{i\omega\mu}\left(\frac{1036}{784}\left(\frac{h_x h_y}{h_z} + \frac{h_y h_z}{h_x}\right) - \frac{h_y h_z}{h_x}\right),$$

$$c_{59} = \frac{269}{5040}h_x h_y h_z \sigma_{rst} - \frac{1}{i\omega\mu}\frac{1036}{784}\left(\frac{h_x h_y}{h_z} + \frac{h_y h_z}{h_x}\right),$$

$$c_{5\,10} = c_{59},$$

$$c_{66} = \frac{781}{5040}h_x h_y h_z \sigma_{rst} + \frac{1}{i\omega\mu}\left(\frac{1036}{784}\left(\frac{h_x h_y}{h_z} + \frac{h_y h_z}{h_x}\right) + \frac{h_y h_z}{h_x}\right) + h_y h_z\left(1-\delta_{rn_x}\right)\beta^{\mathscr{F}}_{rst} + (1-i)\,\delta_{rn_x}h_y h_z a_{rst},$$

$$c_{6\,9} = c_{59},$$

$$c_{6\,10} = c_{5\,10},$$

$$c_{77} = \frac{781}{5040}h_x h_y h_z \sigma_{rst} + \frac{1}{i\omega\mu}\left(\frac{1036}{784}\left(\frac{h_x h_z}{h_y} + \frac{h_y h_z}{h_x}\right) + \frac{h_x h_z}{h_y}\right) + h_x h_z(1-\delta_{s1})\,\beta^{\mathscr{W}}_{rst} + (1-i)\,\delta_{s1}h_x h_z a_{rst},$$

$$c_{78} = \frac{-59}{5040}h_x h_y h_z \sigma_{rst} + \frac{1}{i\omega\mu}\left(\frac{1036}{784}\left(\frac{h_x h_z}{h_y} + \frac{h_y h_z}{h_x}\right) - \frac{h_x h_z}{h_y}\right),$$

$$c_{79} = -\frac{1}{i\omega\mu}h_x,$$

$$c_{7\,10} = \frac{1}{i\omega\mu}h_x,$$

$$c_{7\,11} = \frac{269}{5040}h_x h_y h_z \sigma_{rst} - \frac{1}{i\omega\mu}\frac{1036}{784} \times \left(\frac{h_x h_z}{h_y} + \frac{h_y h_z}{h_x}\right),$$

$$c_{7\,12} = c_{7\,11},$$

$$c_{88} = \frac{781}{5040}h_x h_y h_z \sigma_{rst} + \frac{1}{i\omega\mu}\left(\frac{1036}{784}\left(\frac{h_x h_z}{h_y} + \frac{h_y h_z}{h_x}\right) + \frac{h_x h_z}{h_y}\right) + h_x h_z\left(1-\delta_{sn_y}\right)\beta^{\mathscr{E}}_{rst} + (1-i)\,\delta_{sn_y}h_x h_z a_{rst},$$

$$c_{89} = c_{7\,10},$$

$$c_{8\,10} = c_{7\,9},$$

$$c_{8\,11} = c_{7\,11},$$

$$c_{8\,12} = c_{7\,12},$$

$$c_{99} = \frac{781}{5040}h_x h_y h_z \sigma_{rst} + \frac{1}{i\omega\mu}\left(\frac{1036}{784}\left(\frac{h_x h_y}{h_z} + \frac{h_y h_z}{h_x}\right) + \frac{h_x h_y}{h_z}\right) + h_x h_y(1-\delta_{t1})\,\beta^{\mathscr{S}}_{rst} + (1-i)\,\delta_{t1}h_x h_y a_{rst},$$

$$c_{9\,10} = \frac{-59}{5040} h_x h_y h_z \sigma_{rst} + \frac{1}{i\omega\mu}\left(\frac{1036}{784}\left(\frac{h_x h_y}{h_z} + \frac{h_y h_z}{h_x}\right) - \frac{h_x h_y}{h_z}\right),$$

$$c_{10\,10} = \frac{781}{5040} h_x h_y h_z \sigma_{rst} + \frac{1}{i\omega\mu}\left(\frac{1036}{784}\left(\frac{h_x h_y}{h_z} + \frac{h_y h_z}{h_x}\right) + \frac{h_x h_y}{h_z}\right) + h_x h_y\left(1-\delta_{tn_z}\right)\beta^{\mathcal{N}}_{rst} + (1-i)\,\delta_{tn_z} h_x h_y a_{rst},$$

$$c_{11\,11} = \frac{781}{5040} h_x h_y h_z \sigma_{rst} + \frac{1}{i\omega\mu}\left(\frac{1036}{784}\left(\frac{h_x h_z}{h_y} + \frac{h_y h_z}{h_x}\right) + \frac{h_y h_z}{h_x}\right) + h_y h_z(1-\delta_{r1})\,\beta^{\mathcal{B}}_{rst} + (1-i)\,\delta_{r1} h_y h_z a_{rst},$$

$$c_{11\,12} = \frac{-59}{5040} h_x h_y h_z \sigma_{rst} + \frac{1}{i\omega\mu}\left(\frac{1036}{784}\left(\frac{h_x h_z}{h_y} + \frac{h_y h_z}{h_x}\right) - \frac{h_y h_z}{h_x}\right),$$

$$c_{12\,12} = \frac{781}{5040} h_x h_y h_z \sigma_{rst} + \frac{1}{i\omega\mu}\left(\frac{1036}{784}\left(\frac{h_x h_z}{h_y} + \frac{h_y h_z}{h_x}\right) + \frac{h_y h_z}{h_x}\right) + h_y h_z\left(1-\delta_{rn_x}\right)\beta^{\mathcal{F}}_{rst} + (1-i)\,\delta_{rn_x} h_y h_z a_{rst}.$$

Recall that the lengths h_x, h_y and h_z depend on the indices r, s, and t, respectively; this was not explicitly written for the sake of simplicity. The Kronecker deltas in the definition of the c_{ij}s are included to write in the same expression terms contributing either on Γ, the border of the domain Ω, or inside it. The coefficient a_{rst} that appears in the former, according to its definition below, Eq. (4), has the form $a_{rst} = (\sigma_{rst}/2\,\omega\mu)^{1/2}$.

We mentioned above that β is a complex iteration parameter defined *on* the rectangles building Γ_{rst} with a positive real part and a negative imaginary part, which is a requirement for the algorithm to guarantee uniqueness of the solution and for the iterative algorithm to converge (Douglas et al., 2000). We defined β to be an average of the values of the coefficients a_{rst} on both sides of any given interface times $(1-i)$. With this choice Eq. (12) resembles the absorbing boundary condition (6) for the interior boundaries. It is still an open question if another choice for β can diminish the number of iterations for the algorithm to converge.

Finally, the 12-element vector building the right-hand side of the linear system of equations, at the $n+1$ iteration level has the following form:

$$b^n_{rst} = \begin{pmatrix}
(1-\delta_{s1})\,h_x h_z\left(\beta^{\mathcal{W}}_{rst}\varepsilon^{\mathcal{E}_x,n}_{rs-1t} - \lambda^{\mathcal{E}^n}_{rs-1t,x}\right)\\
\left(1-\delta_{sn_y}\right)h_x h_z\left(\beta^{\mathcal{E}}_{rst}\varepsilon^{\mathcal{W}_x,n}_{rs+1t} - \lambda^{\mathcal{W}^n}_{rs+1t,x}\right)\\
(1-\delta_{t1})\,h_x h_y\left(\beta^{\mathcal{S}}_{rst}\varepsilon^{\mathcal{N}_x,n}_{rst-1} - \lambda^{\mathcal{N}^n}_{rst-1,x}\right)\\
\left(1-\delta_{tn_z}\right)h_x h_y\left(\beta^{\mathcal{N}}_{rst}\varepsilon^{\mathcal{S}_x,n}_{rst+1} - \lambda^{\mathcal{S}^n}_{rst+1,x}\right)\\
(1-\delta_{r1})\,h_y h_z\left(\beta^{\mathcal{B}}_{rst}\varepsilon^{\mathcal{F}_y,n}_{r-1st} - \lambda^{\mathcal{F}^n}_{r-1st,y}\right)\\
\left(1-\delta_{rn_x}\right)h_y h_z\left(\beta^{\mathcal{F}}_{rst}\varepsilon^{\mathcal{B}_y,n}_{r+1st} - \lambda^{\mathcal{B}^n}_{r+1st,y}\right)\\
(1-\delta_{s1})\,h_x h_z\left(\beta^{\mathcal{W}}_{rst}\varepsilon^{\mathcal{E}_z,n}_{rs-1t} - \lambda^{\mathcal{E}^n}_{rs-1t,z}\right)\\
\left(1-\delta_{sn_y}\right)h_x h_z\left(\beta^{\mathcal{E}}_{rst}\varepsilon^{\mathcal{W}_z,n}_{rs+1t} - \lambda^{\mathcal{W}^n}_{rs+1t,z}\right)\\
(1-\delta_{l1})\,h_x h_y\left(\beta^{\mathcal{S}}_{rst}\varepsilon^{\mathcal{N}_y,n}_{rst-1} - \lambda^{\mathcal{N}^n}_{rst-1,y}\right)\\
\left(1-\delta_{ln_z}\right)h_x h_y\left(\beta^{\mathcal{N}}_{rst}\varepsilon^{\mathcal{S}_y,n}_{rst+1} - \lambda^{\mathcal{S}^n}_{rst+1,y}\right)\\
(1-\delta_{r1})\,h_y h_z\left(\beta^{\mathcal{B}}_{rst}\varepsilon^{\mathcal{F}_z,n}_{r-1st} - \lambda^{\mathcal{F}^n}_{r-1st,z}\right)\\
\left(1-\delta_{rn_x}\right)h_y h_z\left(\beta^{\mathcal{F}}_{rst}\varepsilon^{\mathcal{B}_z,n}_{r+1st} - \lambda^{\mathcal{B}^n}_{r+1st,z}\right)
\end{pmatrix}$$

The contribution of the source term must of course be added to the vector b^n_{rst}. If an *XY*-polarization is assumed the quantity — $1/4 h_x h_y h_z \sigma_{rst}\ \boldsymbol{E}_{\mathrm{p}}(z_m)$ — where z_m is the mid-point of Ω_{rst-} is added to the first, second, third, and fourth elements. In the case of a *YX*-polarization, the contribution goes to the fifth, sixth, ninth, and tenth elements.

References

Alumbaugh, D.L., Prevost, G.A., Shadid, J.N., 1996. Three-dimensional wide band electromagnetic modeling on massively parallel computers. Radio Sci. 31, 1–23.

Arnold, D.N., Brezzi, F., 1985. Mixed and nonconforming finite

element methods: implementation, postprocessing and error estimates. R.A.I.R.O. Modélisation, Mathématique et Analyses Numérique 9, 7–32.

Douglas, J. Jr., Paes-Leme, P.J., Roberts, J.E., Wang, J., 1993. A parallel iterative procedure applicable to the approximate solution of second order partial differential equations by mixed finite element methods. Numer. Math. 65, 95–108.

Douglas, J. Jr., Hurtado, F., Pereira, F., 1997. On the numerical simulation of waterflooding of heterogeneous petroleum reservoirs. Comput. Geosci. 1, 155–190.

Douglas, J. Jr., Santos, J., Sheen, D., 2000. A nonconforming mixed finite element method for Maxwell's equations. Math. Model Methods Appl. Sci., In press.

Mackie, R.L., Madden, T.H., Wannamaker, P.E., 1993. Three-dimensional magnetotelluric modeling using difference equations—Theory and comparison to integral equation solutions. Geophysics 58 (2), 215–226.

Martinec, Z., 1997. Spectral-finite-element approach to two-dimensional electromagnetic induction in a spherical earth. Geophys. J. Int. 130, 583–594.

Mogi, T., 1996. Three-dimensional modeling of magnetotelluric data using finite element method. J. Appl. Geophys. 35, 185–189.

Nedelec, J.C., 1980. Mixed finite elements in R^3. Numer. Math. 35, 315–341.

Nedelec, J.C., 1982. Eléments finis mixtes incompressibles pour l' équation de Stokes dans R^3. Numer. Math. 39, 97–112.

Newman, G., Alumbaugh, D., 1997. Three-dimensional massively parallel electromagnetic inversion: I. Theory. Geophys. J. Int. 128, 345–354.

Pacheco, P.S., 1997. Parallel Programming with MPI. Morgan Kaufmann.

Santos, J.E., Sheen, D., 1998. Global and parallelizable domain decomposed mixed FEM for 3D electromagnetic modelling. Comp. Appl. Math. 17 (3), 265–282.

Sheen, D., 1997. Approximation of electromagnetic fields: Part I. Continuous problems. SIAM J. Appl. Math. 57, 1716–1736.

Wannamaker, P.E., Stodt, J.A., Rijo, L., 1987. A stable finite element solution for two-dimensional magnetotelluric modelling. Geophys. J. R. Astron. Soc. 88, 277–296.

Wannamaker, P.E., 1991. Advances in 3D magnetotelluric modelling using integral equations. Geophysics 56, 1716–1728.

Xiong, Z., 1992. Electromagnetic modeling of 3-D structures by the method system iteration using integral equations. Geophysics 57 (12), 1556–1561.

Zhdanov, M., Fang, S., 1996. Quasi-linear approximation in 3-D electromagnetic modeling. Geophysics 61 (3), 646–665.

Zhdanov, M.S., Varentsov, I.M., Weaver, J.T., Golubev, N.G., Krylov, V.A., 1997. Methods for modelling electromagnetic fields: results from COMMEMI — the international project on the comparison of modelling methods for electromagnetic induction. J. Appl. Geophys. 37, 133–271.

Zyserman, F.I., Guarracino, L., Santos, J.E., 1999. A hybridized mixed finite element domain decomposed method for two dimensional magnetotelluric modelling. Earth, Planets Space 51 (4), 297–306.